Journal of Magnetic Resonance 200 (2009) 147–152

Contents lists available at ScienceDirect

Journal of Magnetic Resonance

journal homepage: www.elsevier.com/locate/jmr

Communication

Fast MRI coil analysis based on 3-D electromagnetic and RF circuit co-simulation

Mikhail Kozlov *, Robert Turner

Max Planck Institute for Human Cognitive and Brain Research, Stephanstraße 1A, 04103 Leipzig, Germany

ARTICLE INFO

Article history:
Received 27 January 2009
Revised 5 June 2009
Available online 9 June 2009

Keywords:
Radio-frequency (RF) coils
Magnetic resonance imaging (MRI)
Computational electromagnetics

ABSTRACT

To accelerate the analysis of a multi-element MRI coil, a two-way link is used between radiofrequency (RF) circuit and 3-D electromagnetic (EM) simulation tools. In this configuration, only one 3-D EM simulation is required to investigate the coil performance over a range of different tunings, saving considerable computation time. For the purpose of 3-D EM simulation, the coil feed networks and trim capacitors are substituted by 50 Ω ports. The entire coil was tuned in the RF circuit domain, and the near-field profiles of the electric and magnetic field components were then calculated, together with the specific energy absorption ratio (SAR) maps in the 3-D EM domain

1. Introduction

When magnetic fields of 7 T and higher are used for MRI, the ensuing inhomogeneity of RF magnetic ($\mathbf{B_1}$) fields can be reduced using specialized MRI coil designs. The most important of these is multi-channel transmission [1,2]. However MRI coil analysis becomes very complicated in such a configuration, especially when there is significant coupling between coil elements.

In earlier studies, [1,2] MRI RF coil analysis was performed using 3-D electromagnetic (EM) tools based on finite element methods (FEM), finite difference time domain methods (FDTD), the method of moments (MOM) and some 3-D EM hybrid approaches. The current rapid development of novel 3-D EM tools [3–5], as well as the significant improvement of those already available, makes it difficult to predict which will be optimal for MRI coil design in the near future. Selection of the tools can be made on the basis of available computer hardware and human body models. However, use of 3-D EM tools alone becomes a severe limiting factor in the performance optimization of a multi-element MRI coil when the human body model is included in the simulation domain, because the full highly complex 3-D EM problem must be solved for each tuning condition.

In most cases, a MRI coil is designed and simulated independently of any supporting circuitry (e.g. feed, tuning, and decoupling networks, etc.). In a typical 3-D EM simulation, only the radiative coil elements are represented. When a set of idealized inputs are entered, the $\mathbf{E}$ and $\mathbf{B_1}$ fields, and the SAR profiles, as well as the S parameter matrix, can be simulated. It is common practice to use the 3-D EM domain simulation results – the coil S parameter matrix – in RF circuit analysis [6] but without feedback to the 3-D EM domain. The weakness of this methodology is that the actual 3-D field profiles, which depend on the interaction between the feed network and the coil, are not observable until the physical hardware has been built. This is a less than ideal time for modifications to be made. Changes at this point can be costly and time consuming.

One of the most significant developments in field solver technologies is the creation of a two-way link between RF circuit and 3-D EM simulation tools [7,8]. This enables simulation results from the RF circuit domain to be used to drive the 3-D EM domain. The two-way link is a built-in feature (with varying degrees of flexibility from MRI coil design point of view) in the RF simulation bundles delivered by several vendors (e.g. Ansoft, CST, Agilent, etc.). It is included mainly for the purposes of telecommunication antenna designers, who routinely use it for optimization of antenna array 2-D far field performance. They adjust the parameters of feed networks using RF circuit tools, followed by recalculation (based on RF circuit simulation data) of the far field using the 3-D EM tools.

3-D MRI RF coil design entails near-field simulation, and the coil feed and tuning networks are often independent circuits. As a result, the two-way link approach requires 3-D EM simulation with many more independent ports than are usual in telecommunication antenna development. It also entails the recalculation of 3-D near-field data at many more points in space than 2-D far-field data. Furthermore, the tuning network is not referenced to ground, as it is for the feed network. For this reason, the tuning network must be represented by differential ports, instead of the single-ended ports representing the feed network for telecommunication applications. It must be pointed out that all available vendor-provided implementations of this two-way link have some limitations, such as maximum number of mesh elements, lengthy calculation time, difficulty of handling differential ports, expensive licenses. This inhibits the straightforward use of the two-way link for multi-port MRI coil analysis.

* Corresponding author. Fax: +49 34199402448.
E-mail address: kozlov@cbs.mpg.de (M. Kozlov).

1090-7807/$ - see front matter © 2009 Elsevier Inc. All rights reserved.
doi:10.1016/j.jmr.2009.06.005

Perhaps the absence of turn-key solutions compatible with MRI coil design, with a realistic price, is the reason that the two-way link has not been previously explored by MRI coil designers. In our work, a flexible vendor-independent usage of the two-way link allows optimization of the coil analysis workflow, with a simultaneous reduction of the cost of simulation tool licenses.

2. Method

The two-way link approach relies on the fact that for linear RF networks and a given frequency $\boldsymbol{w}$, the 3-D EM field data are exactly the same in each of the following cases:(a) the RF network is part of a 3-D EM model analyzed by 3-D EM tools; and (b) all the RF networks with negligible mutual coupling are substituted by 3-D EM ports with impedance $\boldsymbol{Z}^j_{port}(\omega)$ (could be, for instance, 50 Ω), and with electromotive force ($\boldsymbol{V}^j(\omega)$) defined for each port as

$$\boldsymbol{V}^j(\omega) = \boldsymbol{I}^j(\omega) \cdot \boldsymbol{Z}^j_{port}(\omega) - \boldsymbol{U}^j_{network}(\omega) \tag{1}$$

where j is port index, $\boldsymbol{U}^j_{network}(\omega)$ is the network cross voltage and $\boldsymbol{I}^j(\omega)$ is the network output current. $\boldsymbol{U}^j_{network}(\omega)$ and $\boldsymbol{I}^j(\omega)$ are calculated in the RF circuit domain, when the network is connected to the corresponding port of an object described by S parameter matrix, obtained by the 3-D EM model simulation.

A workflow diagram of the approach proposed is shown in Fig. 1. After the layout of a coil has been completed using 3-D EM tools, the coil is modified by substitution of all lumped elements required for tuning, feeding and/or decoupling with equivalent ports with impedance of 50 Ω, the standard for MRI scanner feed networks. 3-D EM simulation of this derived multiport design provides $\mathbf{E}^j$ and $\mathbf{B}^j_1$ field prototypes for each simulated port, assuming that the port power amplitude $P^j_{prototype} = 1$ W, with $\varphi^j_{prototype} = 0$ (in most EM tools), and also the multi-port S parameter matrix. This matrix constitutes the source data for an S parameter simulation block enabling design of the RF circuit, together with other parts of scanner RF subsystem and the coil networks of lumped elements for tuning, feeding and/or decoupling. Each coil network is then connected to the corresponding ports of the S parameter simulation block. For a specific tune and feed condition, the RF circuit tool calculates electrical values (resistance, capacitance, inductance, cable length, etc.) of any unknown elements using an optimization procedure, followed by simulation of the electrical properties of the circuit (current and voltage for circuit nodes, S parameter, etc.). The current and voltage values thus obtained for each S parameter simulation block node are used for calculation of $\boldsymbol{V}^j(\omega)$ according to Eq. (1). In most 3-D EM tools the port excitation for combining the results of the multiport simulation is defined by power ($P^j_{port}(\omega)$) and phase ($\varphi^j(\omega)$) rather than by $\boldsymbol{V}^j(\omega)$. We may write, in Matlab notation

$$P^j_{port}(\omega) = |\boldsymbol{V}^j(\omega) \cdot conj(\boldsymbol{V}^j(\omega))/(8 * \boldsymbol{Z}^j_{port})|/P^j_{prototype} \tag{2}$$

$$\varphi^j(\omega) = phase(\boldsymbol{V}^j(\omega)) - \varphi^j_{prototype} \tag{3}$$

The procedure for combining results consists of linear superposition of $\mathbf{E}^j$ and $\mathbf{B}^j_1$ weighted by the P^j_{port} and φ^j provided for each port. This procedure may be executed outside of the EM tools environment using external software such as Matlab. The coil $\mathbf{E}$ and $\mathbf{B}_1$ fields may then be written

$$\mathbf{B}_1 = \sum_j^N \mathbf{B}^j_1 \cdot \sqrt{P^j_{port}(\omega)} \cdot \exp(i\varphi^j(\omega)) \tag{4}$$

$$\mathbf{E} = \sum_j^N \mathbf{E}^j \cdot \sqrt{P^j_{port}(\omega)} \cdot \exp(i\varphi^j(\omega)) \tag{5}$$

where N is the total number of ports.

As a result, the $\mathbf{E}$ and $\mathbf{B}_1$ field profiles for any tune/feed/decoupling condition can be calculated on the basis of only one 3-D EM simulation, together with as many RF circuit analyses as required. The 3-D EM computation is extremely time consuming, especially when high spatial resolution is required, whilst the circuit simula-

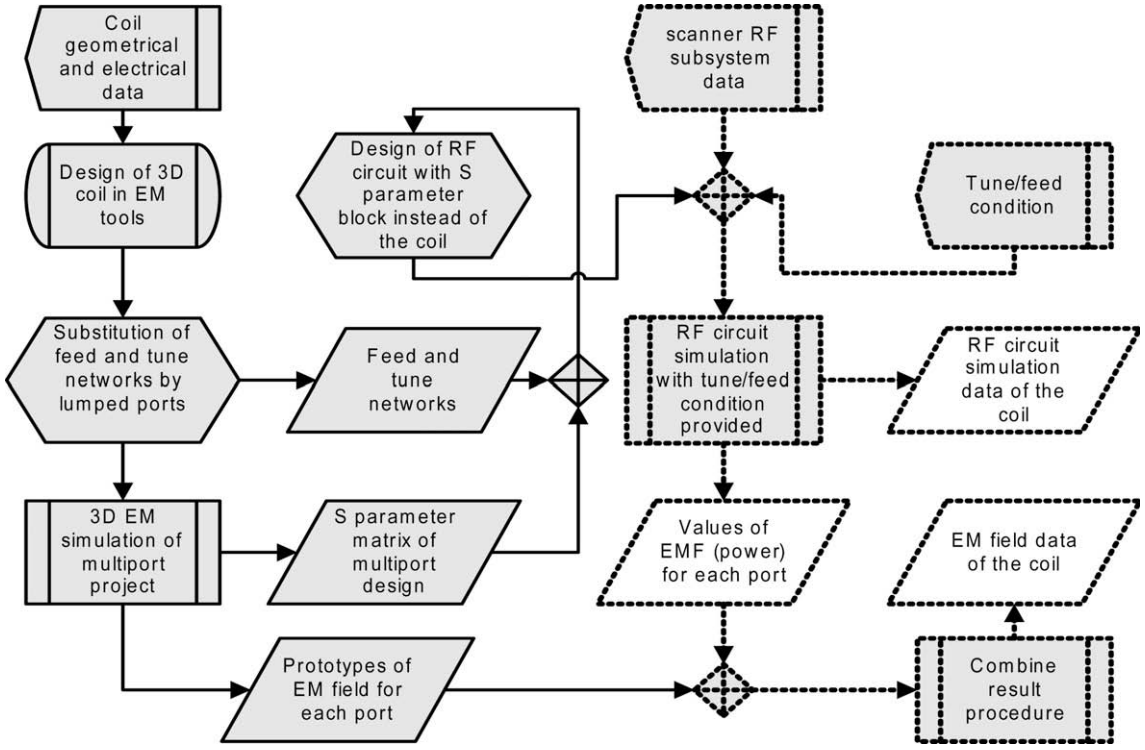

Fig. 1. Workflow of the approach proposed. Solid line is used for operations and paths that are executed only once for a coil design investigated, dotted line is used for operations and paths that can be executed repeatedly to obtain data corresponding to different tune and feed conditions.

tion is quite fast, because RF circuit analysis requires significantly less computer resources than any 3-D EM simulation approach which must deal with a precisely specified realistic human body model. The computation time for the combined result procedure is linearly dependent on the number of mesh elements and ports, and is not significantly time consuming.

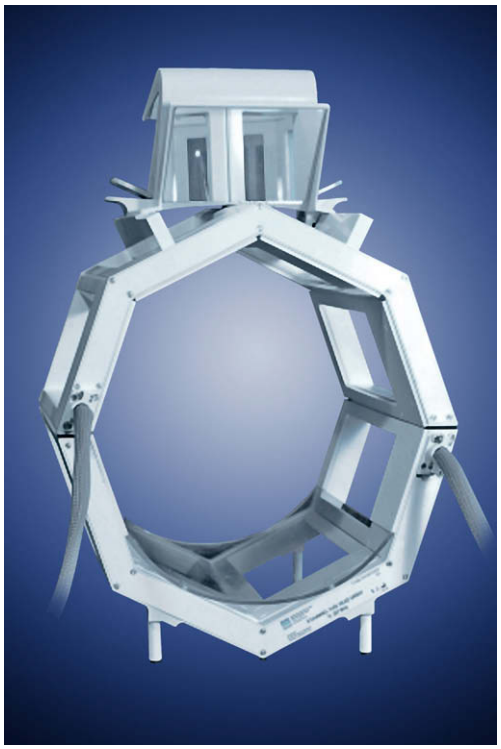

Fig. 2. Rapid 7 T coil.

3. Results

The approach described above has been used as the basis for investigation of the performance of a commercially available Rapid Biomed (RAPID Biomedical GmbH, Technology Park Würzburg-Rimpar, Germany) 7 T 8-element head coil [9] (Fig. 2). The coil inner diameter is 235 mm, outer diameter is 310 mm, and the coupling between neighboring elements $\boldsymbol{S_{xy}} \approx 7$ dB.

In a bench experiment, the electrical properties (S parameter matrixes) of all parts of the coil were measured using a network analyser Agilent E5061A. The frequency (f_{elem}) at which the magnetic field for each element approaches its maximum was measured by connecting an RF source to the coil input and monitoring the output of a shielded coaxial loop placed in the geometrical centre of each element ($\boldsymbol{S}_{21}$ measurement setup). The frequency at which each element's reflection coefficient ($\boldsymbol{S_{xx}}$) approaches its minimum (f_{min_Sxx}) was measured by direct connection to each element input with simultaneous termination of other elements by 50 Ω loads. In further work, MRI measurements of the $\mathbf{B}_1$+ fields actually produced by this coil were performed using a Siemens 7T scanner.

In numerical studies, Agilent ADS was used as the RF circuit tool, CST Microwave Studio (CST) and Ansoft HFSS were each used as 3-D EM tools, and Matlab was used in post-processing. The coil 3-D EM model includes all construction details for the resonance elements, simulated with realistic dimensions and material electrical properties. For each coil element, the RF feed network and trim capacitor, which is on the opposite side to the element's feed point, were substituted with 50 Ω ports. This gave a total number of ports as high as 16.

In the CST simulation the number of mesh cells was increased manually, by changing the mesh resolution for the coil elements,

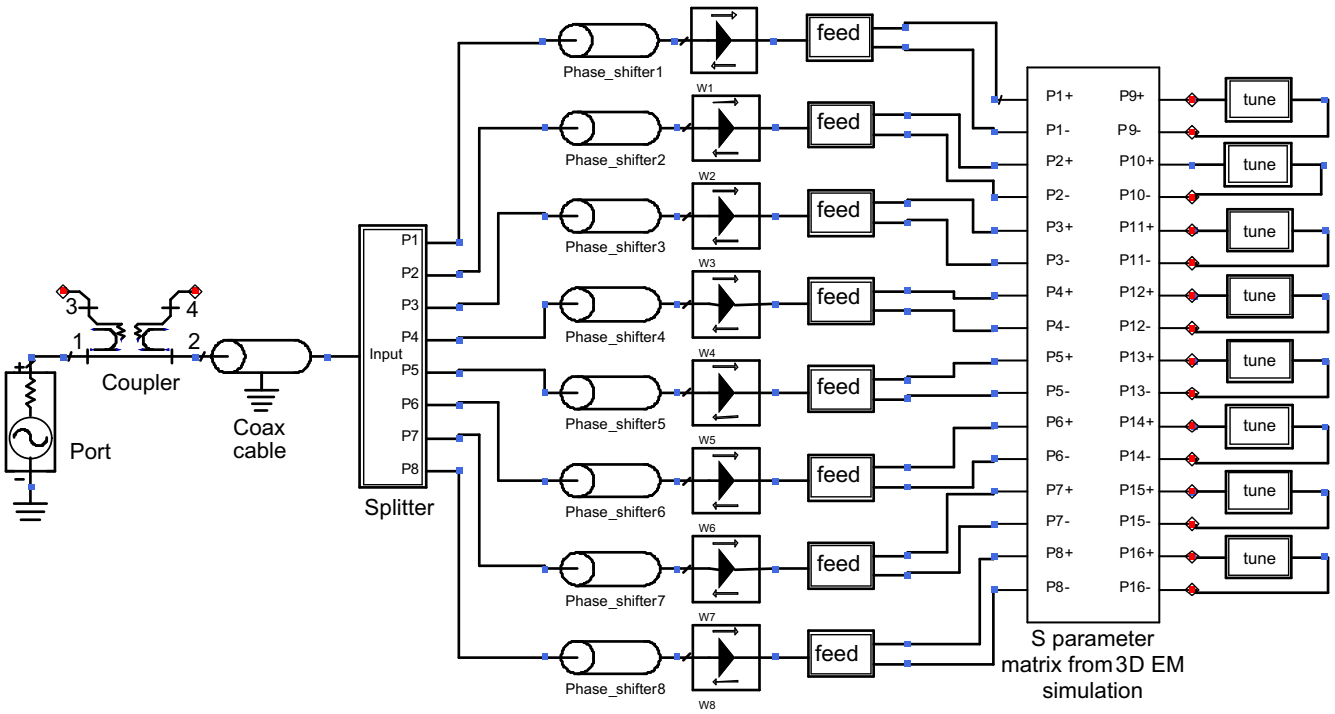

Fig. 3. RF circuit simulation for the coil investigated. Coupler, bi-directional coupler installed at position of Siemens scanner reference plane; Coax cable, summary of several coaxial cables used between the scanner reference plane and the splitter; Splitter, zero phase-difference power splitter; Phase shifter, eight phase shifters (coax cables with well defined length), with preset phase shift for each coil channel; Feed, feed sub-network of fixed lumped capacitors; Tune, tune sub-network of one trim capacitor; W1···W8 – "WaveProbe" for calculation of delivered and reflected power.

until there was no significant difference between the simulated and experimental trim capacitor values obtained using the RF circuit simulation step. This condition was achieved with a 1 mm isotropic mesh size, with a total of 57.2 million mesh nodes. By contrast, HFSS simulation does not require manual adjustment of the mesh size, because it includes a reliable multistep mesh adaptation algorithm, guided by simulation coverage criteria. The final mesh attained using the HFSS simulation for the coil investigated consisted of 2 million tetrahedra. Detailed analysis of the influence of mesh size and mesh adaptation procedure in CST and HFSS on co-simulation data will be published separately.

After the multi-port characterization was obtained by both 3-D EM tools for 50 MHz frequency sweep, the trim capacitors and RF feed networks were connected to these ports for modelling with Agilent ADS. The circuit presented on Fig. 3 includes as in reality: one power source, the coaxial cable, the 8-channel power splitter (with losses as measured for the real splitter but partially idealized, assuming frequency-independent 50 Ω input and output impedances), eight coaxial cable-based phase shifters, and the coil itself. In additional eight wave probes were used numerically to obtain transmitted and reflected power for each coil element. The losses in the coaxial cable were set equal to the measured losses between the scanner power reference plane and the coil splitter.

Most RF circuit tools support both *S* parameter and alternating current (AC) signal simulations. Because the feed network of the coil investigated is based on fixed capacitors, the Agilent ADS *S* parameter optimization procedure was used to obtain only the trim capacitor values for tuning conditions defined by the vendor, which includes minimization of each element's $\boldsymbol{S_{xx}}$ at the MRI resonance frequency of 297.2 MHz (f_{res}) when a water based phantom is placed inside the coil (e.g. all $f_{min\_Sxx} = f_{res}$). As with a bench experiment, such optimization required reconfiguration of the original RF circuit. The power source and the splitter were removed and an individual simulation port was connected to each input phase shifter. Numerical tuning of the coil, with eight port simulation and minimization of $\boldsymbol{S_{xx}}$ (where x varies from 1 to 8) at $f_{res,}$ required about 100 iterations for reliable trim capacitor value definition. This number increased when the numerical value obtained was far away from the experimental value used as a starting point. This was the case for the first CST simulation with 2.5 mm isotropic mesh size.

AC simulation and optimization allows evaluation and tuning of the frequency dependence of the transmitted and reflected power, and the current value in different locations, using the wave and the current probes correspondently. The location of the current probe for the tune circuit is shown in Fig. 4. Current probe data were used for rapid estimation of f_{elem}, because the magnetic field generated by each coil element is defined by the current through it. Values of current flows in the coil through the feed network, and the current through the trim capacitor, are important for understanding coil performance, since a significant variation in current amplitude along the coil explains why the $\mathbf{B}_1$+ profile is asymmetrical in both coronal and sagittal planes.

With the tuning provided by the vendor – such that all $f_{min\_Sxx} = f_{res}$, the ensuing large frequency shift between f_{elem} and f_{res} results in suboptimal coil performance, as shown in Fig. 5. Different alternative tuning conditions were investigated. These were: (a) all $f_{elem} = f_{res}$; (b) P_{ref_coil} approaches its minimum at f_{res}; and some

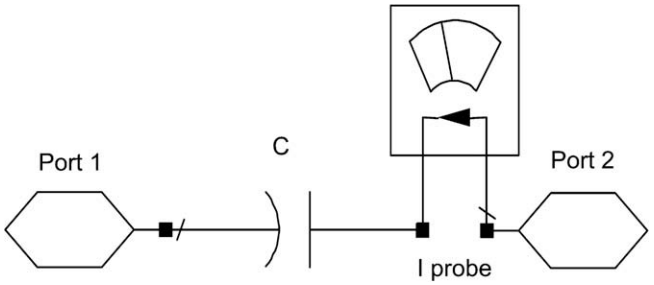

Fig. 4. Sub-network for tune circuit.

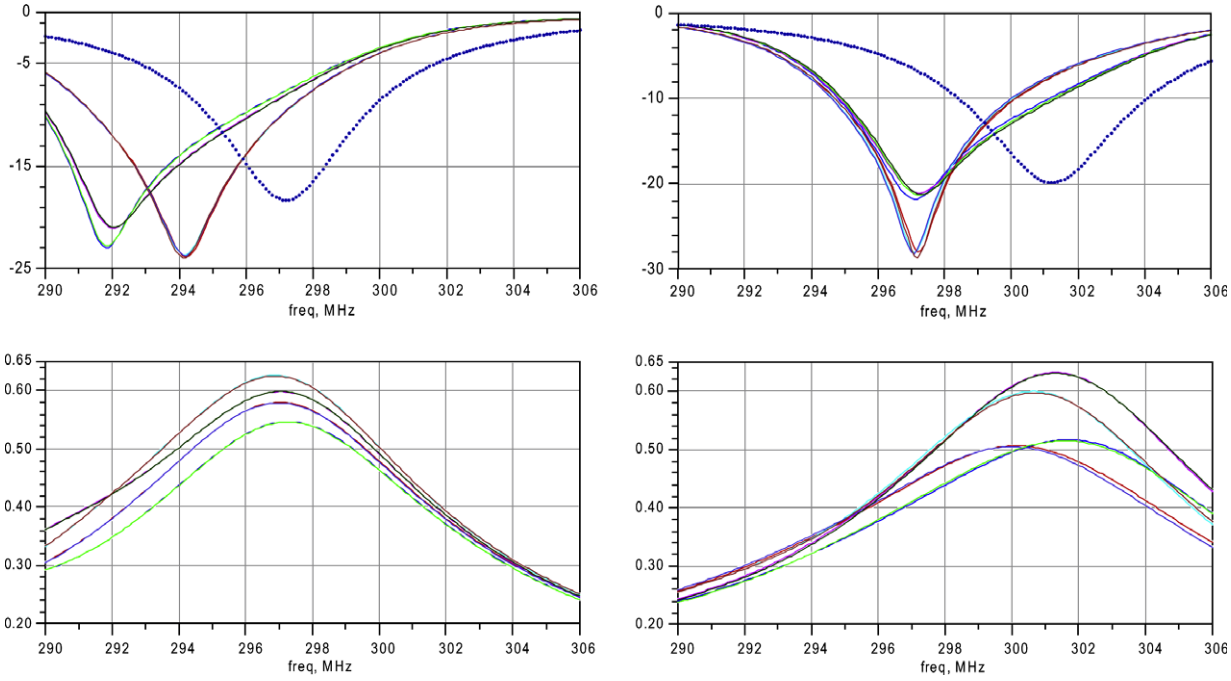

Fig. 5. (top) Power reflected by each coil element (solid lines) and power reflected by entire coil (dotted line). (bottom) current through trim capacitor. (left) P_{ref_coil} minimized at f_{res} = 297.2 MHz, right, f_{min_Sxx} set to be equal to f_{res} = 297.2 MHz.

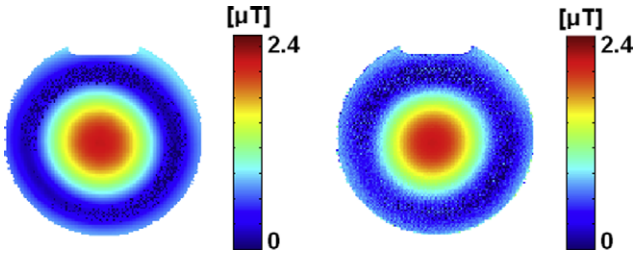

Fig. 6. $\mathbf{B}_1$+ maps of a saline phantom with permittivity equal to 79.5 and conductivity equal to 0.46. Left simulation data, right experimental data mapped experimentally by Insko's double angle method [12].

other tuning arrangements. The first tuning, obtained by an AC optimization procedure, required that the maximum value of the current through each tune capacitor approaches its maximum at f_{res}. The second tuning was obtained by AC minimization at f_{res} of the reflected power by the entire coil, derived as the sum of the reflected power from each coil element as obtained by the wave probes.

Simulation data confirms that the coil's magnetic field approaches a maximum when P_{ref_coil} is minimized. By coil re-tuning, P_{ref_coil} at f_{res} was reduced from more than 43% of transmitted power to less than 11%, with simultaneous increases of as much as 33% for $\mathbf{B}_1$+. The fixed values of the coil feed network capacitors made it impossible to obtain smaller levels of P_{ref_coil}. By numerical adjustment of the feed network capacitors, P_{ref_coil} could be minimized further, until less than 0.4% of transmitted power.

For the two tuning arrangements tested – vendor-provided, and P_{ref_coil} minimized at f_{res} – and two coil loads – saline- and oil-based phantoms – the RF circuit simulation results (S parameter matrix, element-specific Q factors, f_{elem}'s) and 3-D EM simulation results ($\mathbf{B}_1$+ profile) were both found to be almost equal to the corresponding observed data for the RF coil. Simulated and measured $\mathbf{B}_1$+ profiles are shown in Fig. 6. Since the simulated $\mathbf{B}_1$+ data is based on the complete scanner RF subsystem, from power reference plane to coil radiative element, the results can be quantitatively compared [1], not only for the shape of the $\mathbf{B}_1$+ profile, but also the volume performance of the MRI coil, defined as the ratio of the RF field magnitude at any given point to the RF voltage applied at the scanner reference plane. The close agreement between simulated and measured MRI coil volume performance, obtained when the coil was loaded by several phantoms with different size and electrical properties, was limited only by uncertainties in the geometrical and electrical properties provided by the vendors for the MRI scanner RF drive train and the coil, as well as by uncertainties of phantom electrical properties and phantom position inside the coil.

Analysis of the RF amplitude and phase for each substituted feed network port showed that amplitude values and the phase distribution vary significantly from what would be expected in the ideal case (Table 1). This underlines the importance of inclusion of the power splitter and phase shifters in the analysis of 3-D field and SAR data.

Table 1
Power amplitude and phase for each coil input after port substitution by the feed capacitor network, when loaded by a phantom or HUGO. The "ideal case" represents the value if the influence of the feed network is neglected.

Coil element		1	2	3	4	5	6	7	8
Amplitude (W)	Phantom	0.87	0.82	0.87	1	0.87	0.82	0.87	1
	HUGO	0.97	0.81	0.77	0.88	0.86	0.92	0.94	1
	Ideal case	1	1	1	1	1	1	1	1
Phase (°)	Phantom	2	49	101	141	2	49	101	141
	HUGO	4	49	100	137	0	49	96	137
	Ideal case	0	45	90	135	0	45	90	135

Since the coil investigated cannot be easily retuned when installed at an MRI scanner, its in vivo performance was analyzed using mesh definition and trim capacitor values borrowed from the study of the water-based phantom. To change the simulation object from the phantom to a head model corresponds to experimental substitution of the phantom by an in vivo subject inside the tuned-and-matched MRI coil. The Ansoft human body and HUGO models (each with a range of different scaling factors: 1, 0.9, 0.8) and also all models of the "Virtual Family" data set [10] were used. The voxel-based HUGO and "Virtual Family" models were used only in CST simulations because HFSS cannot handle the voxel-based model format.

The two-way link enables one 3-D EM simulation to be sufficient for investigation of the SAR behaviour, for each human body model used, and a range of tuning and feeding conditions that includes transmit array excitation. SAR profiles for the "Ella" and "Billie" models from the "Virtual Family" are presented in Fig. 7. A detailed report of SAR worst case analysis based on these research data will be published separately.

3-D EM simulation times were about 32 days for CST (with the final mesh) and 2 days for HFSS, when a single high-end PC desktop computer was used. If port simulation parallelization is used in CST, or frequency sweep point simulation parallelization is used in HFSS, the corresponding simulation time will be reduced linearly, proportional to the number of computers used for parallelization. For the final mesh condition, numerical tuning would have been completely unfeasible using only the 3-D EM tools. Using the two-way link approach, tuning itself was performed within minutes in Agilent ADS.

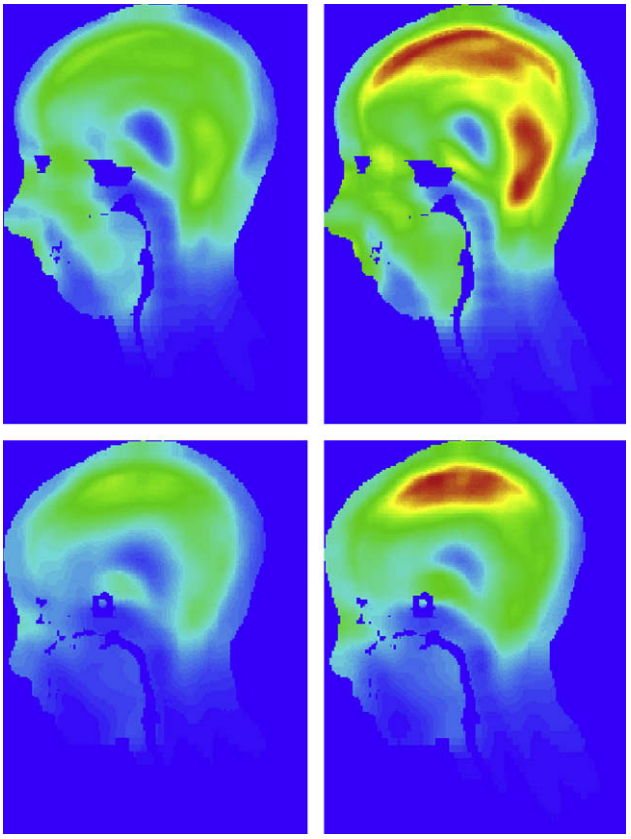

Fig. 7. Ten gram SAR. Top "Ella", bottom "Billie" models of "Virtual Family" human body data set. Left, P_{ref_coil} minimized at f_{res}, right, f_{min_Sxx} set to be equal to f_{res}. Max SAR value for "Ella" – 1.71 W/kg, for "Billie" – 2.70 W/kg. Colour scale of left and right plots are the same. Transmit power is 8 W.

The tuning-guided recalculation of both **E** and $\mathbf{B}_1$ field data, followed by data saving to dedicated files, took about 25 min for a 57.2 million mesh CST project. This time was mostly devoted to reading and writing field data files larger than 1 GB. The HFSS post-processing workflow does not require production of internal separate field data files for specific individual port amplitude and phase conditions. Any field based calculations or export to an ASCII-based file are performed by the HFSS field calculator "on-the-fly" using the actual port conditions provided by the user. The exported HFSS data were used for performing SAR calculations in Matlab.

4. Discussion

The concept of introducing ports at the locations of lumped element networks during 3-D EM simulation has more general application in high field MRI coil design. For instance, there are no analytical expressions to estimate the capacitance values of distributed capacitors, as commonly used in birdcage coils and the decoupling networks of multi-channel coils. While these values can be estimated in principle by optimization with the 3-D EM simulator [11], they can be computed much more rapidly by co-simulation, when the two-way link is used with a 3-D EM simulator for which the simulation time is not significantly dependent on the number of simulated ports (as it is true for Ansoft HFSS).

For most commercial 3-D EM tools, it should be noted that substitution of an RF network by a lumped 3-D EM port which is not a true differential port imposes constraints on the behavior of the *S* parameter objects of the RF circuit with differential ports. The incoming current through the plus terminals must be the same as the current leaving through the minus terminals. This is true for most tuning and feeding networks used for MRI coil design.

For the frequency range used in MRI (below 500 MHz), the important initial assumption of negligible mutual coupling between each substituted network is not an issue, when the distributed and trim capacitors are physically small and separated by distances many times longer than their largest dimension. For some MRI coil designs, capacitive coupling between feed networks might be apparently significant, but since this issue is important for the MRI coil operation itself, reliable solutions are normally used in which such coupling is cancelled, using appropriate connections between feed network and radiative coil element (for instance, using cable traps, etc.). This allows simulation of the feed network as described above.

This approach was validated by performing a number of simulations for the coil analyzed where the feed and tune networks were not substituted by ports. The results of these simulations for the optimized feed and tune capacitor values were exactly the same as for the corresponding port substitution simulations. The maximum difference of $\mathbf{B}_1$+ and SAR 3-D data between these simulations was less than 0.5%.

MRI safety guidelines define a maximum allowable SAR for in vivo MRI scanning, and a coil factor (K) – the ratio of SAR to absorbed coil power ($P_{absorbed}$) – which is used for computing the SAR during an MRI scan. Scanner software can estimate $P_{absorbed}$ only from real-time measurements of transmitted ($P_{transmit}$) and reflected ($P_{reflect}$) power data obtained at the scanner's RF power reference plane, together with losses measured previously between the scanner power reference plane and the coil input.

When a multi-element coil is driven using power splitters that absorb the power reflected by the coil (i.e. $P_{reflect} \approx 0$) which is the case for the Rapid 7 T coil, SAR safety monitoring becomes more complex, because the correct $P_{absorbed}$ cannot be obtained in real-time. SAR safety monitoring that takes into account K and only $P_{transmit}$ overestimates SAR, a significant drawback for MRI scanner performance.

When simulation is sufficiently precise to give no visible difference between the measured and simulated data in both simulation domains, use of SAR to $P_{transmit}$ ratio is reliable enough to guarantee SAR safety monitoring, since the behaviour of the entire RF MRI scanner subsystem, from power reference plane to coil, is thus demonstrated to be properly understood.

Using simulations with different human models, multi-element coil tuning can be pre-adjusted to provide the best possible performance for a given head mass and shape distribution without retuning for every subject. This somewhat complex optimization procedure can be implemented in Matlab, for instance.

5. Conclusions

Despite the fact that computer power and memory have increased significantly over the last few years, the available 3-D EM tools still do not allow treatment of complete design problems that include complex RF sub-circuits (RF cable, power splitter, phase shifter, etc.), and they are far from optimal for performance optimization of a coil with adjustable lumped elements and a complex load.

The two-way link-based RF circuit and 3-D EM co-simulation method offers a reliable and fast workflow for multi-element coil analysis with a human model as load. Designers can then not only simulate both the feed network and the MRI coil as a single system, but also obtain 3-D EM field data and SAR for different feed/tuning conditions without rerunning the very time consuming 3-D simulation.

Vendor-independent usage of the two-way link allows use of only one RF tool with several different 3-D EM tools, achieving desirable flexibility of analysis workflow with a simultaneous reduction of the cost of simulation tool licenses.

References

[1] G. Adriany, P.F. van de Moortele, F. Wiesinger, Transmit and receive transmission line array for 7T parallel imaging, Magn. Reson. Med. 53 (2000) 434–445.
[2] T.S. Ibrahim, L. Tang, Insight into RF power requirements and B1 field homogeneity for human MRI via rigorous FDTD approach, J. Magn. Reson. Imaging 25 (6) (2007) 1235–1247.
[3] B.K. Li, F. Liu, E. Weber, S. Crozier, Hybrid numerical techniques for the modelling of radiofrequency coils in MRI, NMR Biomed. (2008) (published online).
[4] S. Wang, J.H. Duyn, Time-domain finite-difference/finite-element hybrid simulations of radio frequency coils in magnetic resonance imaging, Phys. Med. Biol. 53 (2008) 2677–2692.
[5] P.J. Cassidy, S. Grieve, K. Clarke, D.J. Edwards, Electromagnetic characterisation of RF coils using the Transmission Line Modelling (TLM) method, Proc. Int. Soc. Mag. Reson. Med. 9 (2001) 693.
[6] E. Boskamp et al., Efficiency of a 3T whole body 16 channel TEM transmit array, Proc. Int. Soc. Mag. Reson. Med. 16 (2008) 1094.
[7] K. Guillouard, M.-F. Wong, V.F. Hanna, J. Citerne, A new global finite element analysis of microwave circuits including lumped elements, IEEE Trans. Microw. Theory Technol. 44 (2006) 2287–2594.
[8] D. Bailargeat, E. Larique, S. Verdeyme, M. Aubourg, R. Sommet, P. Guillon, Coupled localized and distributed element analysis applying an electromagnetic software in frequency domain, in: G.A. Koepf (Ed.), IEEE MTS-S International Microwave Symposium Digest, New York, 1997, pp. 1021–1024.
[9] A. Weisser, T. Lanz, A volume head array with 8 transmit/Receive Channels for 7 T, Proc. Int. Soc. Mag. Reson. Med. 14 (2006) 2591.
[10] A. Christ et al., The virtual family – development of anatomical CAD models of two adults and two children for dosimetric simulations. Available from: <http://www.itis.ethz.ch/index/index_humanmodels.html>.
[11] B. Wu, X. Zhang, P. Qu, G.X. Shen, Design of an inductively decoupled microstrip array at 9.4 T, J. Magn. Reson. 182 (2006) 126–132.
[12] E.K. Insko, L. Bolinger, Mapping of the radiofrequency field, J. Magn. Reson. 103 (1993) 82–85.

射 频 和 天 线 设 计 培 训 课 程 推 荐

易迪拓培训(www.edatop.com)由数名来自于研发第一线的资深工程师发起成立，致力并专注于微波、射频、天线设计研发人才的培养；我们于 2006 年整合合并微波 EDA 网(www.mweda.com)，现已发展成为国内最大的微波射频和天线设计人才培养基地，成功推出多套微波射频以及天线设计经典培训课程和 ADS、HFSS 等专业软件使用培训课程，广受客户好评；并先后与人民邮电出版社、电子工业出版社合作出版了多本专业图书，帮助数万名工程师提升了专业技术能力。客户遍布中兴通讯、研通高频、埃威航电、国人通信等多家国内知名公司，以及台湾工业技术研究院、永业科技、全一电子等多家台湾地区企业。

易迪拓培训课程列表：http://www.edatop.com/peixun/rfe/129.html

射频工程师养成培训课程套装

该套装精选了射频专业基础培训课程、射频仿真设计培训课程和射频电路测量培训课程三个类别共 30 门视频培训课程和 3 本图书教材；旨在引领学员全面学习一个射频工程师需要熟悉、理解和掌握的专业知识和研发设计能力。通过套装的学习，能够让学员完全达到和胜任一个合格的射频工程师的要求…

课程网址：http://www.edatop.com/peixun/rfe/110.html

ADS 学习培训课程套装

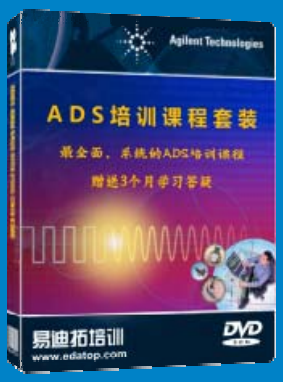

该套装是迄今国内最全面、最权威的 ADS 培训教程，共包含 10 门 ADS 学习培训课程。课程是由具有多年 ADS 使用经验的微波射频与通信系统设计领域资深专家讲解，并多结合设计实例，由浅入深、详细而又全面地讲解了 ADS 在微波射频电路设计、通信系统设计和电磁仿真设计方面的内容。能让您在最短的时间内学会使用 ADS，迅速提升个人技术能力，把 ADS 真正应用到实际研发工作中去，成为 ADS 设计专家...

课程网址： http://www.edatop.com/peixun/ads/13.html

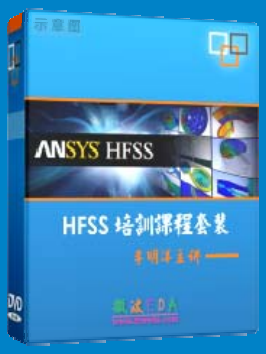

HFSS 学习培训课程套装

该套课程套装包含了本站全部 HFSS 培训课程，是迄今国内最全面、最专业的 HFSS 培训教程套装，可以帮助您从零开始，全面深入学习 HFSS 的各项功能和在多个方面的工程应用。购买套装，更可超值赠送 3 个月免费学习答疑，随时解答您学习过程中遇到的棘手问题，让您的 HFSS 学习更加轻松顺畅…

课程网址：http://www.edatop.com/peixun/hfss/11.html

CST 学习培训课程套装

该培训套装由易迪拓培训联合微波 EDA 网共同推出，是最全面、系统、专业的 CST 微波工作室培训课程套装，所有课程都由经验丰富的专家授课，视频教学，可以帮助您从零开始，全面系统地学习 CST 微波工作的各项功能及其在微波射频、天线设计等领域的设计应用。且购买该套装，还可超值赠送 3 个月免费学习答疑…

课程网址：http://www.edatop.com/peixun/cst/24.html

HFSS 天线设计培训课程套装

套装包含 6 门视频课程和 1 本图书，课程从基础讲起，内容由浅入深，理论介绍和实际操作讲解相结合，全面系统的讲解了 HFSS 天线设计的全过程。是国内最全面、最专业的 HFSS 天线设计课程，可以帮助您快速学习掌握如何使用 HFSS 设计天线，让天线设计不再难…

课程网址：http://www.edatop.com/peixun/hfss/122.html

13.56MHz NFC/RFID 线圈天线设计培训课程套装

套装包含 4 门视频培训课程，培训将 13.56MHz 线圈天线设计原理和仿真设计实践相结合，全面系统地讲解了 13.56MHz 线圈天线的工作原理、设计方法、设计考量以及使用 HFSS 和 CST 仿真分析线圈天线的具体操作，同时还介绍了 13.56MHz 线圈天线匹配电路的设计和调试。通过该套课程的学习，可以帮助您快速学习掌握 13.56MHz 线圈天线及其匹配电路的原理、设计和调试…

详情浏览：http://www.edatop.com/peixun/antenna/116.html

我们的课程优势：

※ 成立于 2004 年，10 多年丰富的行业经验，

※ 一直致力并专注于微波射频和天线设计工程师的培养，更了解该行业对人才的要求

※ 经验丰富的一线资深工程师讲授，结合实际工程案例，直观、实用、易学

联系我们：

※ 易迪拓培训官网：http://www.edatop.com

※ 微波 EDA 网：http://www.mweda.com

※ 官方淘宝店：http://shop36920890.taobao.com